

Local damage detection of a fan blade under ambient excitation by three-dimensional digital image correlation

Yujia Hu^{1a}, Xi Sun^{1b}, Weidong Zhu^{*2} and Haolin Li^{1c}

¹School of Mechanical Engineering, University of Shanghai for Science and Technology, Shanghai 200093, China

²Department of Mechanical Engineering, University of Maryland, Baltimore County, 1000 Hilltop Circle, Baltimore, MD 21250, USA

(Received June 13, 2019, Revised August 2, 2019, Accepted August 16, 2019)

Abstract. Damage detection based on dynamic characteristics of a structure is one of important roles in structural damage identification. It is difficult to detect local structural damage using traditional dynamic experimental methods due to a limited number of sensors used in an experiment. In this work, a non-contact test stand of fan blades is established, and a full-field noncontact test method, combined with three-dimensional digital image correlation, Bayesian operational modal analysis, and damage indices, is used to detect local damage of a fan blade under ambient excitation without use of baseline information before structural damage. The methodology is applied to detect invisible local damage on the fan blade. Such a method has a seemingly high potential as an alternative to detect local damage of blades with complex high-precision surfaces under extreme working conditions because it is a noncontact test method and can be used under ambient excitation without human participation.

Keywords: three-dimensional digital image correlation; Bayesian operational modal analysis; local damage detection

1. Introduction

Blades with complex surfaces are widely used in aerospace, automobile, and electric power industries. However, it is difficult to identify their modal parameters especially for some high-precision blades under working conditions, such as aero-engine and helicopter blades. Difficulties are mainly reflected in the following aspects: (1) strict test conditions are demanded. Traditional contact test methods cannot be used in extreme working conditions. (2) Input excitation, such as hammer impact, cannot be used to excite blades due to their high-precision requirement. (3) Mass loading of sensors with traditional test methods can affect dynamic test results. Thus, it is important to identify modal parameters of blades under ambient excitation by use of a noncontact test method and detect their local damage.

Digital image correlation (DIC) plays an important role in noncontact measurement in experimental mechanics. Bruck *et al.* (1989) proposed Newton-Raphson optimization algorithm that is one of the most important progresses of DIC. This method not only has high precision, but also quickly converges as long as the initial value of deformation is reasonable. In order to satisfy requirements of three-dimensional (3D) deformation measurement on the surface of a structure, Luo *et al.* (1994) proposed a 3D-DIC method. While the 3D-DIC method is mainly utilized for

displacement and strain measurement and determination of material properties (Schmidt *et al.* 2006, Chevalier *et al.* 2001, Hu *et al.* 2018a, b, c, Ye *et al.* 2015), some works have been devoted to vibration analysis (Beberriss and Ehrhardt 2016, Hagara *et al.* 2012, Zanarini 2018, Ha *et al.* 2015). Full-field vibration measurement methods by use of 3D-DIC are always combined with experimental modal analysis (EMA) (Helfrick *et al.* 2011). Due to difficulty in recording input excitation data when testing structures are high-precision blades or large-scale structures, operational modal analysis (OMA) instead of EMA can be used in 3D-DIC vibration measurement to identify modal parameters of a structure with unknown excitation. One primary advantage of OMA is that only output vibration of a structure needs to be measured. Using 3D-DIC combined with OMA, Poozesh *et al.* (2016) obtained operational mode shapes of turbine blades. However, since DIC measurement has some limitations in modal analysis with a low sampling rate and a short recording-data length due to limitations of cameras, Bayesian OMA (BOMA) is well suited for modal analysis to overcome these difficulties. BOMA adopts a Bayesian identification approach for OMA. Moreover, it is much more convenient to use BOMA than EMA and conventional OMA methods due to the following reasons: (1) it can extract modal parameters of a structure based on only response measurement and it can process response time histories at all measured degrees of freedom (DOFs). Yuen and Katafygiotis (2001) found that only one set of response time histories is required. (2) It can overcome challenges of noisy measurement data and short-length recording data from DIC measurement (Yuen and Katafygiotis 2003, Au *et al.* 2013). (3) It obtains not only optimal values of modal parameters, but also uncertainties and signal-to-noise ratios that can be used to evaluate

*Corresponding author, Professor
E-mail: wzhu@umbc.edu

^a Associate Professor

^b Ph.D. Candidate

^c Professor

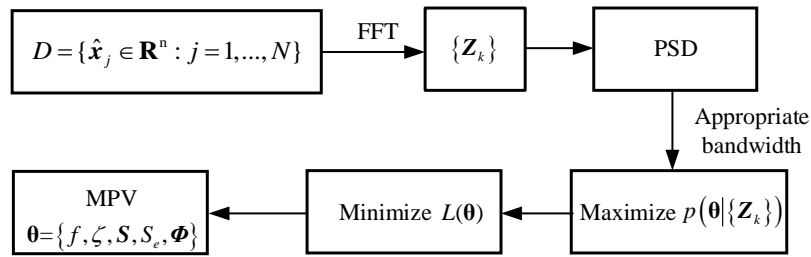


Fig. 1 Flow chart of BOMA

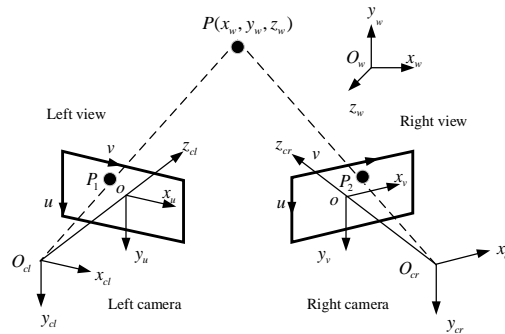


Fig. 2 Binocular stereo vision

analysis results (Au 2011, Au *et al.* 2013).

Modal parameters are often used to detect damage of a structure, such as use of natural frequency shifts (Cawley and Admas 1979), mode shapes and their derivatives (Pandey *et al.* 1991), a damage index based on a modal strain energy (Shi *et al.* 1998, Hu *et al.* 2018), a mode shape damage index (MSDI) (Xu and Zhu 2017), and Gaussian mode shape curvature damage index (Xu and Zhu 2017). It is difficult to locate damage by natural frequency shifts and their sensitivity to damage is not high. Mode shapes and their derivatives are sensitive to local damage. However, numerical differentiation used in analyzing mode shapes would cause misjudgment of damage. Damage indices obtained by different methods are used to more explicitly detect local damage. Such indices often require structural information before and after damage. With the MSDI and Gaussian curvature damage index (GCDI) that do not require structural information before damage (Xu and Zhu 2017, Xu *et al.* 2017), structural damage can be identified in neighborhoods with high values of the MSDI and GCDI. The fundamental idea behind such a method is that a modified mode shape from a polynomial that fits a mode shape obtained by modal identification is regarded as the mode shape of the structure before damage since local damage is assumed to be highly localized, which cannot be captured by a polynomial with a relatively low order.

In this work, a noncontact damage identification method that combines 3D-DIC, BOMA, and the MSDI and GCDI is used to detect invisible local damage of a fan blade without use of baseline information before structural damage. The primary advantage of this method is that it is based on environmental vibration testing without human participation, which has a seemingly high potential as an

alternative to detect local damage of blades with complex high-precision surfaces under extreme working conditions.

2. Background of the theoretical framework of BOMA and 3D-DIC

BOMA (Katafygiotis and Yuen 2001, Yuen and Katafygiotis 2005, Brownjohn *et al.* 2018) adopts a Bayesian identification approach for OMA. Such a method values the traditional fast Fourier transform (FFT) theory as a core and views modal identification as an inference problem in which probability is used as a measure of relative plausibility of outcomes given a model of a structure and measured data central to Bayesian theorem. In particular, BOMA methods are capable of extracting all the information from ambient excitation history data through its posterior statistics and the description method by probability logic better satisfies properties of modal parameters under random excitation. The analysis process of BOMA is introduced as follows: (1) one obtains measured response data $D = \{\hat{x}_j \in \mathbf{R}^n : j=1, \dots, N\}$ of a structure, such as displacements and accelerations. (2) The FFT is performed on the measured data and an augmented vector $\{Z_k\} = [F_k^T, G_k^T]^T \in \mathbf{R}^{2n}$ that contains real and imaginary parts of the FFT results F_k can be defined, where F_k and G_k are real and imaginary parts of F_k , respectively. (3) An appropriate frequency bandwidth near a resonant frequency is selected from power spectral density (PSD) results. (4) A negative log likelihood function $L(\theta)$ can be obtained as an objective optimization function, where θ are modal parameters of a structure, including the natural frequency f , modal damping ratio ζ , mode shape Φ ,

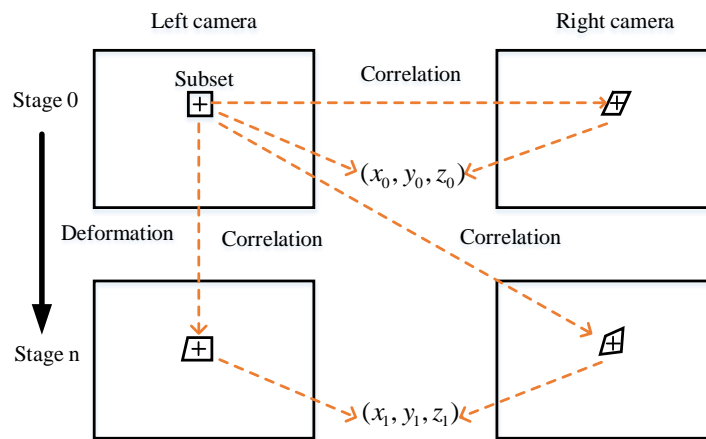


Fig. 3 Schematic of the 3D DIC method



Fig. 4 (a) Speckle pattern and (b) three artificial damage on the fan blade

PSD of the modal force S , and PSD of the prediction error S_e . (5) Minimizing $L(\theta)$, one can obtain the most probable values (MPV) of the modal parameters θ . The flow chart of BOMA is shown in Fig. 1.

3D-DIC is an optical technique that combines binocular stereo vision (Fig. 2) with DIC to measure 3D full-field displacements (Ye *et al.* 2013, Ye *et al.* 2016) on the surface of a structure. Two cameras are used to observe the same object from different perspectives and obtain images at different viewing angles. The triangulation principle is used to calculate offsets among pixels according to the matching relationship between the images, thereby acquiring the 3D information of the object.

A reference image is divided into small rectangular regions or subsets consisting of $N \times N$ pixels. The interval or step between two subsets is a . In this experiment, a subset is adjusted by the size of an analysis area and the step is chosen to be 2. As shown in Fig. 3, the subset to be calculated is selected in the image of the left camera before deformation. The position of the image of the right camera before deformation is found through stereo matching.

According to pre-calibrated internal and external parameters of the cameras, 3D coordinates (x_0, y_0, z_0) of the center point of the subset of the image before deformation can be obtained. By the same method with use of two images obtained by the left and right cameras after deformation, 3D coordinates (x_1, y_1, z_1) of the center point of the subset of the image after deformation can also be obtained. Displacements of the center point of the subset of the image can be obtained by use of the 3D coordinates before and after deformation. The strain field can be obtained by an appropriate differential calculation method or a smoothing method followed by differential calculation (Hartley and Zisserman 2003, Sutton 1991, Wang 2002, Feng and Rowlands 1987) for 3D displacements.

3. Local damage detection of a fan blade

A damage detection test stand of fan blades is established, and a full-field noncontact test method, combined with 3D-DIC, BOMA, and the MSDIs, is used to detect local damage of a fan blade under ambient excitation

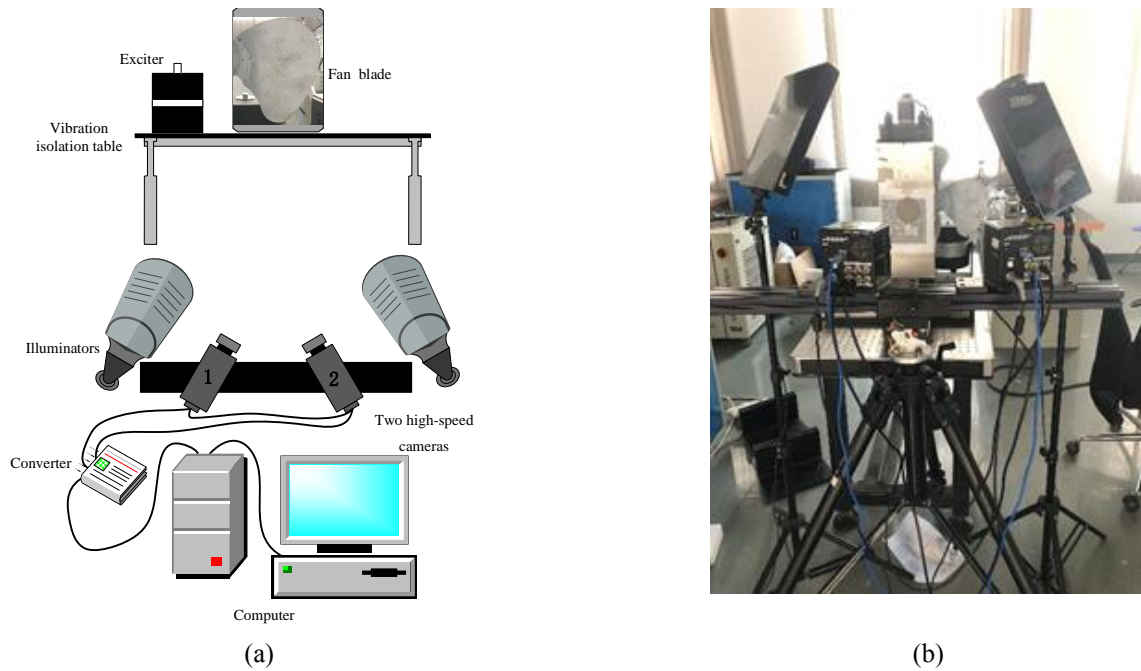


Fig. 5 (a) Schematic and (b) the photo of the experimental setup

without use of baseline information before structural damage. The experimental equipment mainly consists of a fan blade with a diameter of 400 mm and a thickness of 0.7 mm, two high-speed cameras, two illuminators, and an exciter that can provide ambient excitation in a laboratory condition. The center of the fan blade is fixed on the test stand. The distance between the cameras and fan blade is about 660 mm. In order to increase contrast of the speckle pattern in Fig. 4(a) and improve the test accuracy, a matte white paint is used to whiten the surface of the fan blade. According to the resolution of the cameras and size of the photographed area, an appropriate size of the speckle pattern is selected to print a uniformly black spot with a moderate density on the surface of the fan blade. A random speckle with a diameter of 0.5 mm is used in this work. Three artificial local damage with different locations and sizes is made on the back surface of the fan blade, which is invisible in front of the blade, as shown in Fig. 4(b), where the first and second local damage is triangles with a base of 10 mm and a height of 5 mm, and a base of 5 mm and a height of 2.5 mm, respectively. The third local damage is approximately a circle with a radius of 5 mm, as shown in Fig. 4(b). The depth of each damage is about 0.4 mm. Two Photron high-speed cameras, each with a resolution of up to 1280×1024 pixels, and a Nikon lens (AF 28 mm/2.8D) were used to capture images at a frame rate of 2000 f/s, which is sufficient to analyze the first few natural frequencies of the fan blade. The experimental setup for the fan blade is shown in Fig. 5.

The first undeformed fan blade image is used as the reference image, and the rest images are deformed fan blade images. By 3D-DIC, one can obtain time-history curves of out-of-plane displacements at different measurement points on the fan blade, as shown in Fig. 6, where the number of subsets is 27. It can be seen that the maximum amplitude of

the displacements is nearly 0.15 mm, which is sufficiently small so as not to increase damage of the fan blade. Figs. 7(a) and 7(b) show PSDs and singular-value spectra of different measurement points of the fan blade, respectively. It is difficult to select peaks from the PSDs due to inappropriately scaled abscissa. Thus, the singular-value spectra are given from FFT results of the displacements. Peaks can be easily selected from the singular-value spectra, where three peaks can be obviously seen near 15 Hz, 23 Hz, and 35 Hz in the 0~50 Hz frequency range. Note that measured natural frequencies are those of the entire system that includes the fan blade and its surrounding fixture. The three measured natural frequencies may not be the first three natural frequencies of the fan blade because the exciter is used to excite the test stand. Natural frequencies of the test stand that can cause severe disruption for local damage of the fan blade can be recorded in Figs. 7(a) and 7(b). In order to more accurately judge whether the peaks in Figs. 7(a) and (b) correspond to natural frequencies of the fan blade, an accelerometer is used to test natural frequencies of the fan blade. Excitation on the fan blade is weak, which does not excite much the test stand. Fig. 7(c) shows PSDs of signals obtained by the accelerometer. Frequency bandwidths of the fan blade from Figs. 7(a)-7(c) can be easily identified. The validity of measured displacements can be indirectly guaranteed according to comparison between Figs. 7(a) and 7(c), which are PSDs of displacement data obtained from acceleration data measured by 3D-DIC and the high-accuracy acceleration sensor, respectively. One can find that natural frequencies of the fan blade are consistent. Hu *et al.* (2019) have also shown that small displacements can guarantee the accuracy and precision of out-of-plane displacement measurement. The first and second frequency bandwidths are about 15-20 Hz and 35-40 Hz, respectively. The first and second natural

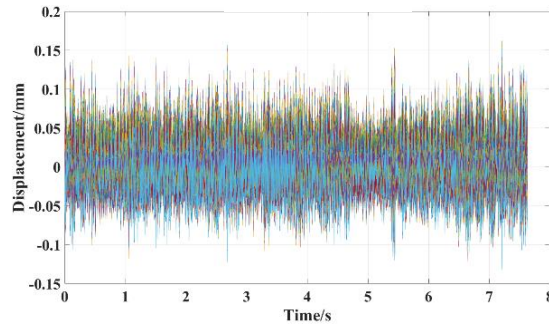


Fig. 6 Time-history curves of out-of-plane displacements at different measurement points on the fan blade

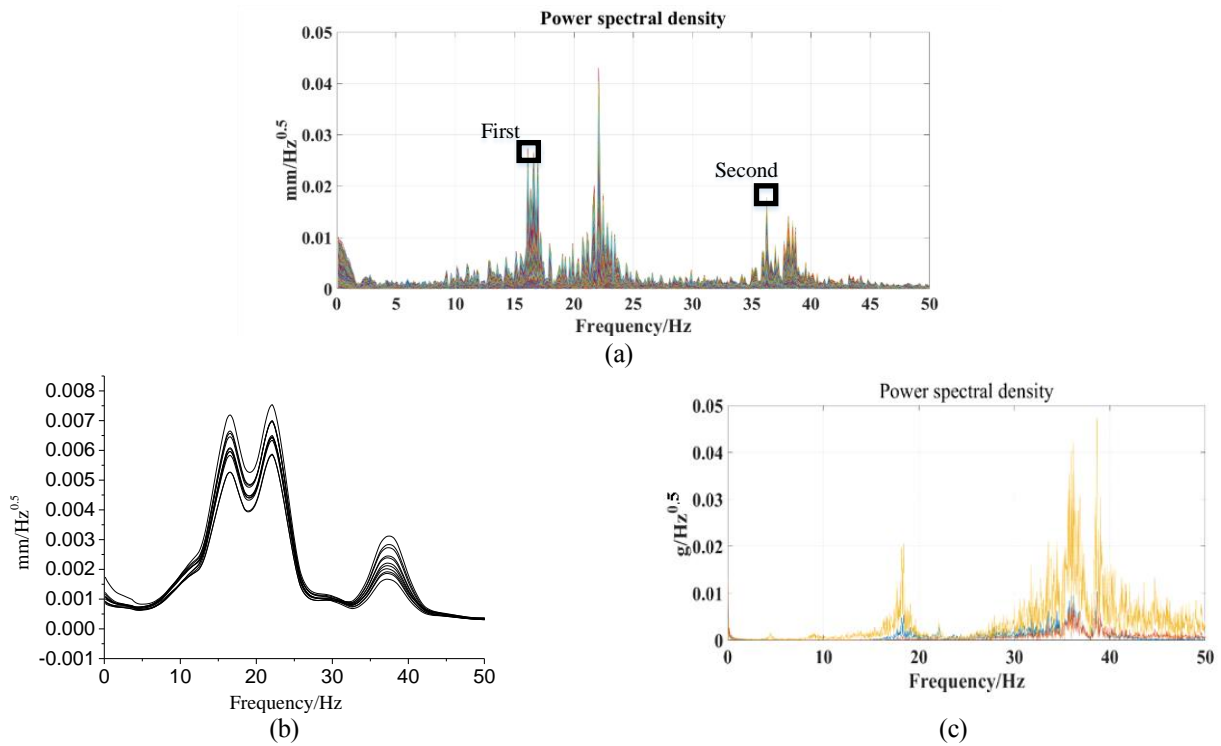


Fig. 7 (a) PSDs obtained by 3D-DIC, (b) the singular-value spectrum of the fan blade, and (c) PSDs obtained by an accelerometer

Table 1 Identified modal parameters of the fan blade

Mode	$f(\text{Hz})$	$\zeta(\%)$	$S(10^{-5}\text{mm}^2/\text{Hz})$	$S_e(10^{-7}\text{mm}^2/\text{Hz})$	γ
1	16.13	0.0024	1.01	5.45	538308.2
2	36.25	0.0105	4.19	19.5	48359.2

frequencies of the fan blade are predicted to be 17 Hz and 37 Hz, respectively. By BOMA, one can obtain the first and second modal parameters of the fan blade, as shown in Table 1 and Fig. 8.

In order to detect the damage from the identified mode shapes of the fan blade, the MDSI and GCDI are used in this work. They are defined by

$$\delta(\mathbf{p}) = (\mathbf{Z}^{d,j}(\mathbf{p}) - \mathbf{Z}^{u,j}(\mathbf{p}))^2 \quad (1)$$

$$\delta^{\text{Gaussian}}(\mathbf{p}) = (\mathbf{G}_{\mathbf{Z}^{d,j}}(\mathbf{p}) - \mathbf{G}_{\mathbf{Z}^{u,j}}(\mathbf{p}))^2 \quad (2)$$

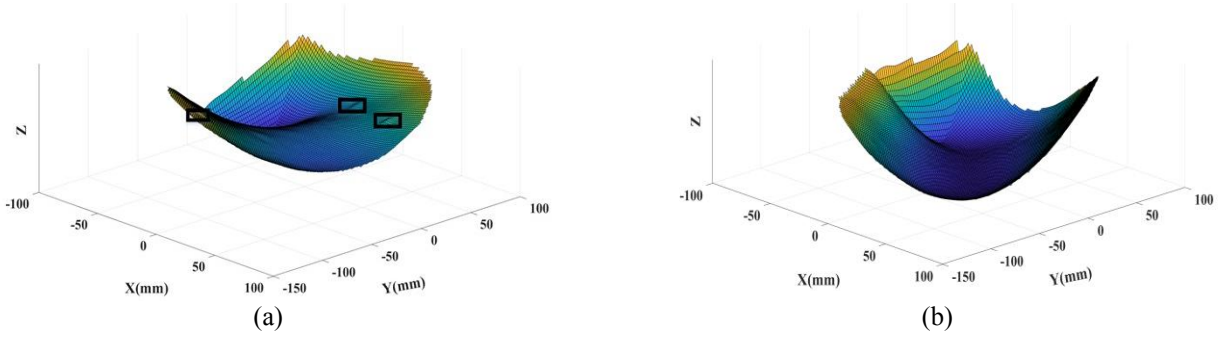


Fig. 8 (a) First and (b) second mode shapes of the fan blade

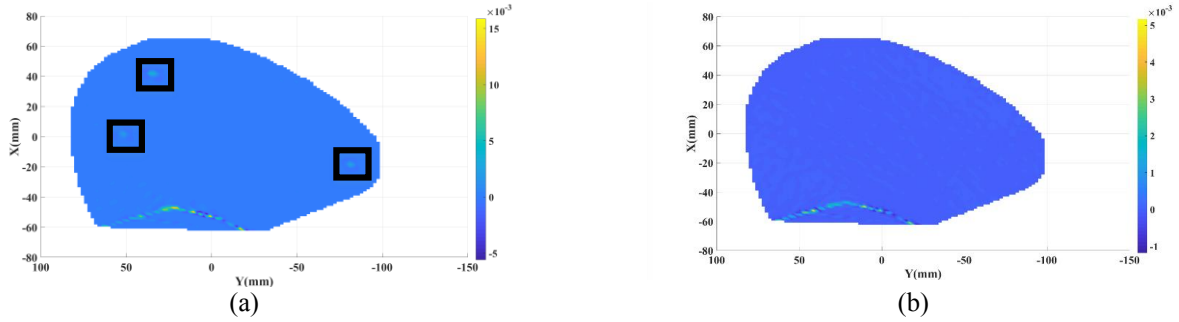


Fig. 9 (a) First and (b) second Gaussian curvature mode shapes of the fan blade

respectively, where \mathbf{p} is a position vector that can be described by coordinates x and y , $\mathbf{Z}^{dj}(\mathbf{p})$ and $\mathbf{G}_{Z^{dj}}(\mathbf{p})$ are the j -th mode shape and Gaussian mode shape curvature of a structure after damage, respectively; and $\mathbf{Z}^{uj}(\mathbf{p})$ and $\mathbf{G}_{Z^{uj}}(\mathbf{p})$ are the j -th mode shape and Gaussian mode shape curvature of a structure before damage, respectively. Gaussian curvatures $\mathbf{G}_{Z^{dj}}(\mathbf{p})$ and $\mathbf{G}_{Z^{uj}}(\mathbf{p})$ are uniformly represented as $\mathbf{G}_{Z,p}$, which can be expressed as

$$\mathbf{G}_{Z,p} = \kappa_{Z,p}^{Max} \times \kappa_{Z,p}^{Min} \quad (3)$$

where $\kappa_{Z,p}^{Max}$ and $\kappa_{Z,p}^{Min}$ are the maximum and minimum values of $\kappa_{Z,p}(\mathbf{v}) = -(\nabla_{\mathbf{v}} \mathbf{n}) \cdot \mathbf{v}$, in which \mathbf{n} and \mathbf{v} are normal and tangent vectors of \mathbf{p} , respectively. By use of mode shapes in Figs. 8(a) and 8(b) and Eq. (3), the first and second Gaussian curvatures of the fan blade can be obtained, as shown in Figs. 9(a) and 9(b), respectively. It can be seen from Figs. (8) and (9) that the three local damage can be detected by the first mode shape and Gaussian curvature of the fan blade although the damage identification results may not have high quality. However, the three local damage cannot be detected from the second mode shape and Gaussian curvature of the fan blade. The MDSI and GCDI are then used to detect the local damage of the fan blade. It is difficult to obtain mode shapes of a structure and their derivatives before damage. A modified mode shape from a polynomial that fits a mode shape obtained by modal identification is regarded as the mode shape of the structure before damage since local damage is assumed to be highly localized, which cannot be captured by a polynomial with a relatively low order. In order to judge the quality of the fit, a fitting index $fit(n)$ is

introduced. It is defined by

$$fit(n) = \frac{RMS(\mathbf{Z})}{RMS(\mathbf{Z}) + RMS(\mathbf{e})} \times 100\% \quad (4)$$

where \mathbf{e} represents the error between mode shapes and their derivatives before and after the fit for the MSDI and GCDI, respectively, and $RMS(\cdot)$ represents the root mean square value of a vector. The fitting accuracy required in this work is chosen to be at least 99.5%. This means that when the fitting accuracy reaches 99.5%, the current polynomial fitting order can be used for the undamaged mode shape or Gaussian curvature. Figs. 10 and 11 show MSDIs δ and GCDIs $\delta^{Gaussian}$ obtained by the first and second mode shapes of the fan blade, respectively, where the polynomial fitting orders are 16 and 15, respectively. The three local damage can be distinctly detected from the MSDIs δ and GCDIs $\delta^{Gaussian}$ obtained by the first mode shape. However, the three local damage still cannot be detected from the MSDIs δ and GCDIs $\delta^{Gaussian}$ obtained by the second mode shape. It is noted that there are high values of δ and $\delta^{Gaussian}$ at some boundaries of the fan blade, which are caused by polynomial fits at some boundaries of the fan blade. The most important reason that the three local damage cannot be identified by use of the second mode shape of the fan blade is that the second mode shape is not sensitive to the damage. A refined damage identification technique is carried out in this work. Three sub-areas and corresponding coordinate systems near the three damage identified by the first mode shape are given as shown in Fig. 12. 3D-DIC is used to obtain displacements of the three sub-areas of the blade with numbers of subsets being 31, 30, and 33. BOMA is used to identify the second mode shapes of the three sub-

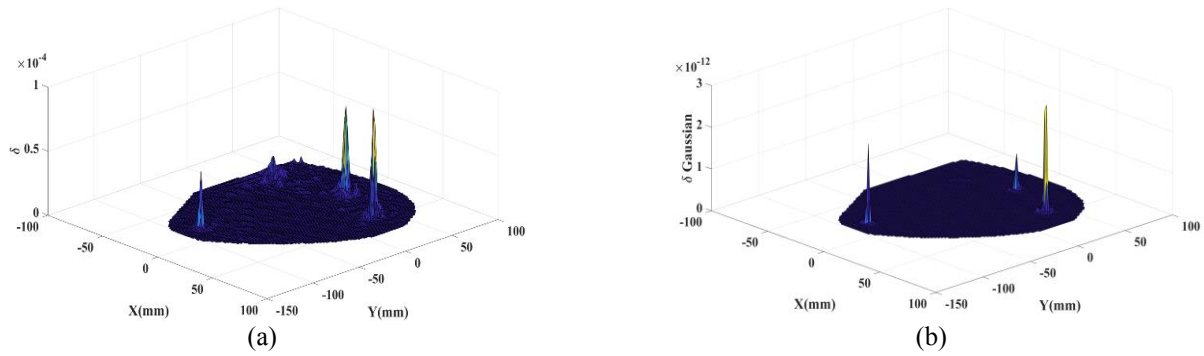


Fig. 10 (a) MSDIs δ and (b) GCDIs $\delta^{Gaussian}$ obtained by the first mode shape of the fan blade

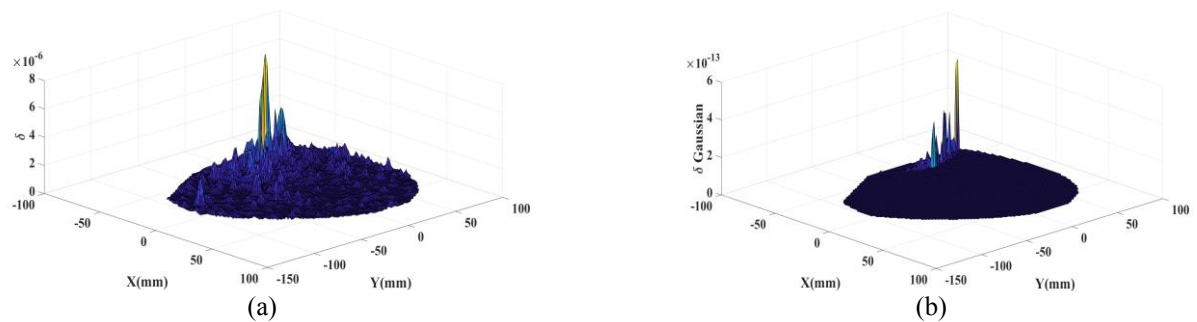


Fig. 11 (a) MSDIs δ and (b) GCDIs $\delta^{Gaussian}$ obtained by the second mode shape of the fan blade

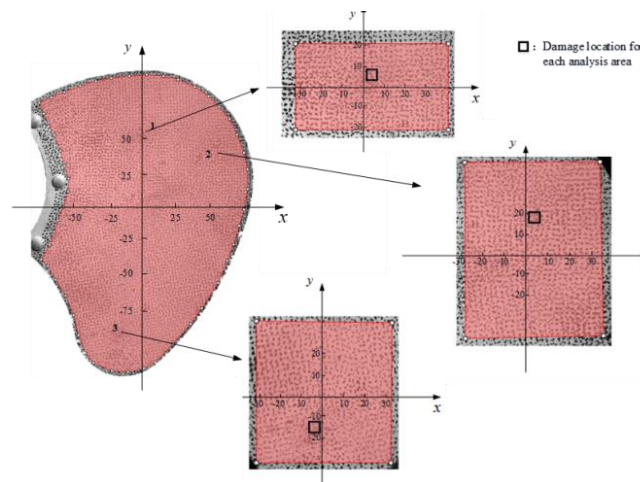


Fig. 12 Sub-areas and coordinate systems near the three damage

areas, as shown in Fig. 13. MSDIs δ and GCDIs $\delta^{Gaussian}$ of the first, second, and third sub-areas of the blade are shown in Figs. 14-16, respectively. It can be found that local damage in the second and third sub-areas can be identified by MSDIs δ and GCDIs $\delta^{Gaussian}$ by use of the second mode shapes of the corresponding sub-areas. However, local damage in the first sub-area still cannot be identified. The reason is that the location of the first damage is almost at the junction of the undeformed shape and second mode shape of the fan blade, which makes the amplitude at the first damage in the second mode shape small, as shown in Fig. 17, where the red denotes the undeformed shape of the

fan blade and the blue the second mode shape of the fan blade. It is noted that the size of the damage to be detected has many influencing factors, such as the size and distribution of speckle patterns, distances between speckles, and the resolution of the cameras. According to the equipment in this work, the smallest damage that can be detected is a local damage with the length being 3-4 mm and the depth 0.3-0.4 mm. The GCDI is more suitable than the MSDI for local damage detection since results with use of the GCDI are more clear and smooth than those with use of the MSDI.

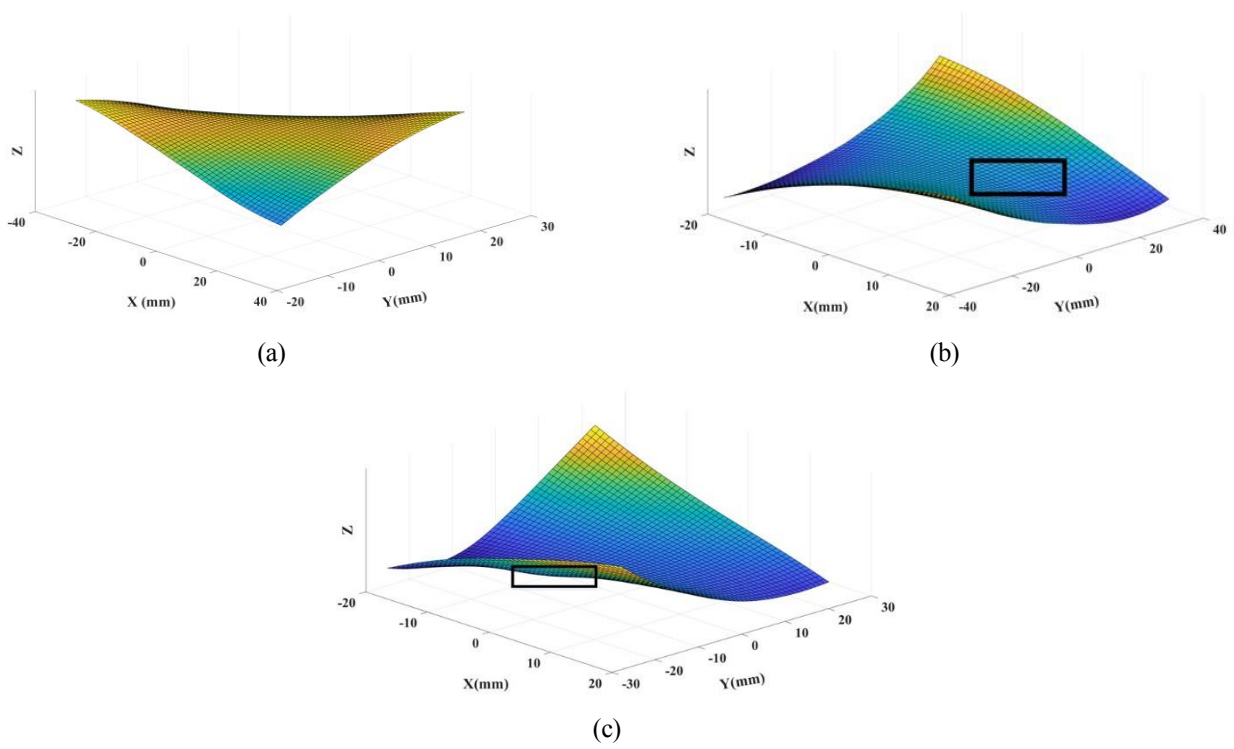


Fig. 13 Second mode shape for the (a) first sub-area, (b) second sub-area, and (c) third sub-area of the fan blade

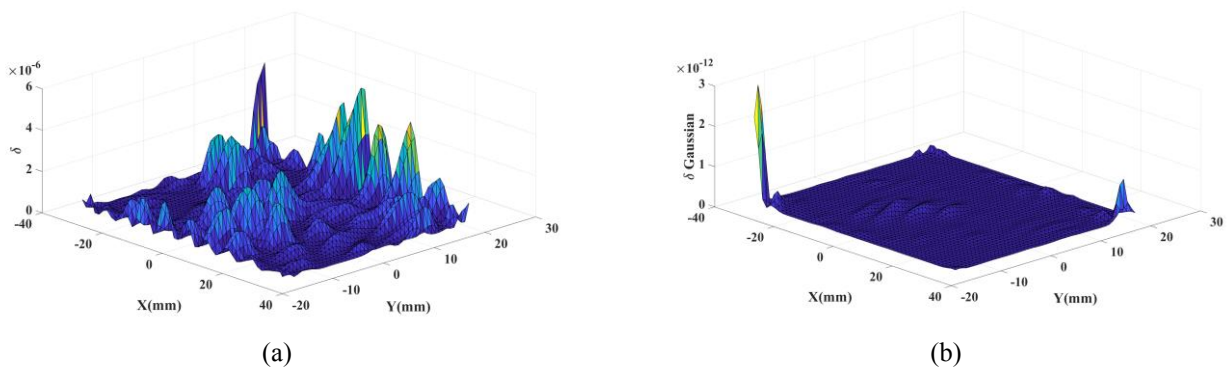


Fig. 14 (a) MSDIs δ and (b) GCDIs $\delta^{Gaussian}$ of the first sub-area of the fan blade

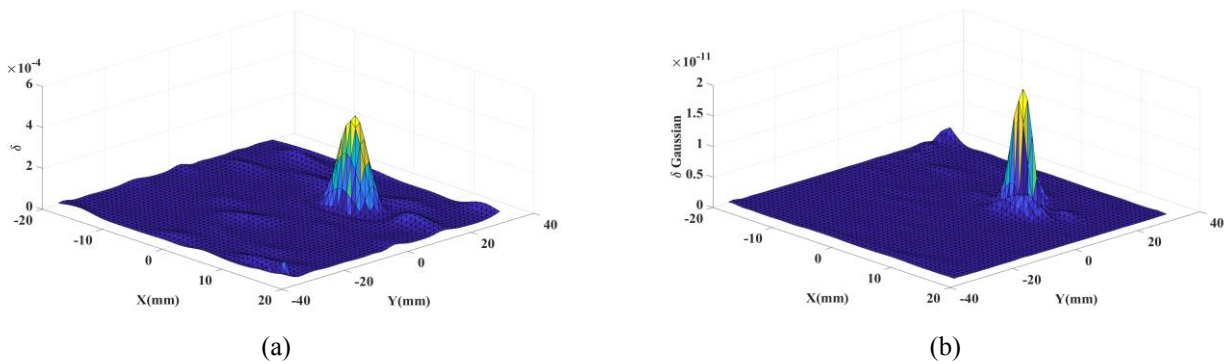


Fig. 15 (a) MSDIs δ and (b) GCDIs $\delta^{Gaussian}$ of the second sub-area of the fan blade

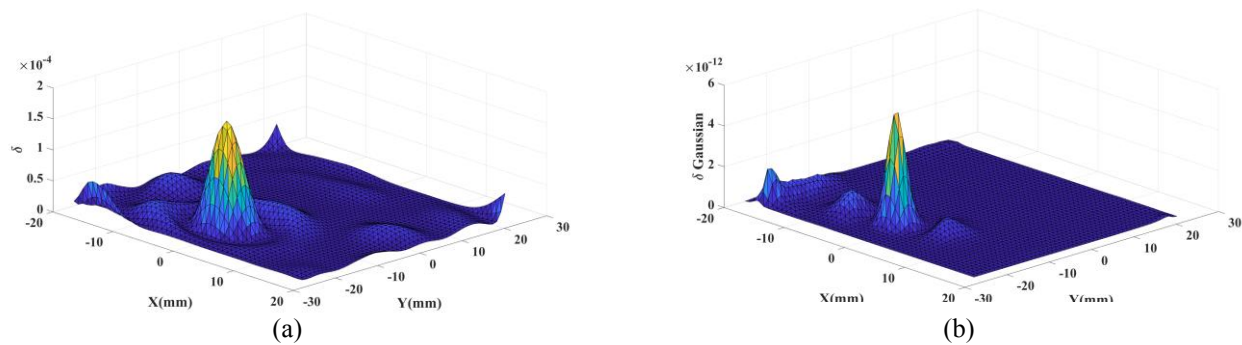


Fig. 16 (a) MSDIs δ and (b) GCDIs $\delta^{Gaussian}$ of the third sub-area of the fan blade

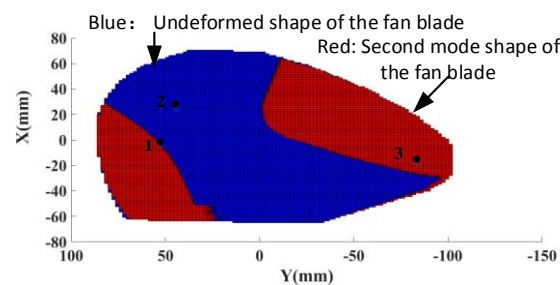


Fig. 17 X-Y view of the undeformed shape and second mode shape of the fan blade

6. Conclusions

A full-field noncontact dynamic test method that combines 3D-DIC and BOMA is proposed to identify modal parameters of a fan blade under ambient excitation. Damage indices such as the MSDI and GCDI obtained by identified mode shapes and their derivatives, respectively, are used to detect invisible local damage of the fan blade without use of baseline information of the blade before damage. Three local damage of the fan blade has been successfully detected. Main advantages of the method are as follows: (1) it can be easily implemented, and (2) it has a seemingly high potential as an alternative to detect local damage of blades with complex high-precision surfaces under extreme working conditions because it is a noncontact test method and can be used under ambient excitation without human participation. However, this method is currently used to detect local damage of a stationary fan blade. One may do further research to detect local damage of a rotating fan blade.

Acknowledgements

The authors would like to thank the financial support from the Shanghai Natural Science Foundation (Project No. 17ZR1419800), Shanghai Science and Technology Innovation Fund (Project No. 17060502600), National Science Foundation (Award No. 1763024), and National Natural Science Foundation of China (Award Nos. 11772100 and 51975379).

References

- Au, S.K. (2011), "Fast bayesian FFT method for ambient modal identification with separated modes", *J. Eng. Mech.*, **137**, 214-226. DOI: 10.1061/(ASCE)EM.1943-7889.0000213.
- Au, S.K., Zhang, F.L. and Ni, Y.C. (2013), "Bayesian operational modal analysis: theory, computation, practice", *Comput. Struct.*, **126**, 3-14. DOI: 10.1016/j.compstruc.2012.12.015.
- Bebernis, T.J. and Ehrhardt, D.A. (2016), "High-speed 3D digital image correlation vibration measurement: recent advancements and noted limitations", *Mech. Syst. Signal Pr.*, **86**, 35-48. DOI: 10.1016/j.ymsp.2016.04.014.
- Brownjohn, J., Au, S., Zhu, Y., Sun, Z., Li, B., Bassitt, J., Hudson, E. and Sun, H. (2018), "Bayesian operational modal analysis of Jiangyin Yangtze River bridge", *Mech. Syst. Signal Pr.*, **110**, 210-230. DOI: 10.1016/j.ymsp.2018.03.027.
- Bruck, H.A., McNeill, S.R., Sutton, M.A. and Peters, W.H. (1989), "Digital image correlation using newton-raphson method of partial differential correction", *Exp. Mech.*, **29**(3), 261-267. DOI: 10.1007/BF02321405.
- Cawley, P. and Admas, R.D. (1979), "The location of defects in structures from measurements of the natural frequencies", *J. Strain Anal.*, **14**(2), 49-57. DOI: 10.1243/03093247V142049.
- Chevalier, L., Calloch, S., Hild, F. and Marco, Y. (2001), "Digital image correlation used to analyze the multiaxial behavior of rubber-like materials", *Eur. J. Mech. A-Solids*, **20**(1), 169-187. DOI: 10.1016/S0997-7538(00)01135-9.
- Feng, Z. and Rowlands, R.E. (1987), "Continuous full-field representation and differentiation of three-dimensional experimental vector data", *Comput. Struct.*, **26**(6), 979-990. DOI: 10.1016/0045-7949(87)90115-5.
- Ha, N.S., Vang, H.M. and Goo, N.S. (2015), "Modal analysis using digital image correlation technique: An application to artificial wing mimicking beetle's hind wing", *Exp. Mech.*, **55**(5), 989-998. DOI: 10.1007/s11340-015-9987-2.

- Hagara, M., Trebuña, F., Huñady, R. and Kalina, M. (2012), "Experimental identification of modal parameters of thin metal sheets by using of DIC", *Procedia Eng.*, **48**(1), 180-188. DOI: 10.1016/j.proeng.2012.09.503.
- Hartley, R. and Zisserman, A. (2003), *Multiple View Geometry in Computer Vision*, Cambridge University Press, Cambridge, UK
- Helfrick, M. N., Niezrecki, C., Avitabile, P. and Schmidt, T. (2011), "3D digital image correlation methods for full-field vibration measurement", *Mech. Syst. Signal Pr.*, **25**(3), 917-927. DOI: 10.1016/j.ymsp.2010.08.013.
- Hu, Y.J., Guo, W.G., Jiang, C. and Zhou Y.L. and Zhu, W.D. (2018), "Looseness localization for bolted joints using Bayesian operational modal analysis and modal strain energy", *Adv. Mech. Eng.*, **10**, 1-10. DOI: 10.1177/1687814018808698.
- Hu, Y.J., Guo, W.G., Zhu, W.D. and Xu, Y. (2019), "Local damage detection of membranes based on Bayesian operational modal analysis and three-dimensional digital image correlation", *Mech. Syst. Signal Pr.*, **131**, 633-648. DOI: 10.1016/j.ymsp.2019.04.051.
- Hu, Y.J., Jiang, C., Liu, W., Yu, Q.Q. and Zhou, Y.L. (2018c), "Degradation of the in-plane shear modulus of structural BFRP laminates due to high temperature", *Sensors*, **18**(10), 1-16. DOI: 10.3390/s18103361.
- Hu, Y.J., Liu, F., Zhu, W.D. and Zhu, J.M. (2018a), "Thermally coupled constitutive relations of thermoelastic materials and determination of their material constants based on digital image correlation with a laser engraved speckle pattern", *Mech. Mater.*, **120**, 26-36. DOI: 10.1016/j.mechmat.2018.02.002.
- Hu, Y.J., Wang, Y.J., Chen, J.B. and Zhu, J.M. (2018b), "A new method of creating high-temperature speckle patterns and its application in the determination of the high-temperature mechanical properties of metals", *Exp Tech.*, **42**, 523-532. DOI:10.1007/s40799-018-0256-z.
- Katafygiotis, L.S. and Yuen, K.V. (2001), "Bayesian spectral density approach for modal updating using ambient data", *Earthq. Eng. Struct. D.*, **30**(8), 1103-1123. DOI: 10.1016/S0266-8920(01)00004-2.
- Luo, P.F., Chao, Y.J. and Sutton, M.A. (1994), "Application of stereo vision to three-dimensional deformation analyses in fracture experiments", *Opt. Eng.*, **33**(3), 981-991. DOI: 10.1117/12.160877.
- Pandey, A.K., Biswas, M. and Samman, M.M. (1991), "Damage detection from changes in curvature mode shapes", *J. Sound Vib.*, **145**(2), 321-332. DOI: 10.1016/0022-460X(91)90595-B.
- Poozesh, P., Baqersad, J., Niezrecki, C. and Avitabile, P. (2016), "A multi-camera stereo DIC system for extracting operating mode shapes of large scale structures", *Conf. Proc. Soc. Exp. Mech. Ser.*, **3**, 225-238. DOI: 10.1007/978-3-319-22446-6_29.
- Schmidt, T.E., Tyson, J. and Galanulis, K. (2006), "Full-field dynamic displacement and strain measurement using advanced 3D image correlation photogrammetry: Part I", *Exp. Mech.*, **27**(3), 47-50. DOI: 10.1111/j.1747-1567.2003.tb00118.x.
- Shi, Z.Y., Law, S.S. and Zhang, L.M. (1998), "Structural damage localization from modal strain energy change", *J. Sound Vib.*, **218**(5), 825-844. DOI: 10.1006/jsvi.1998.1878.
- Sutton, M.A. (1991), "Full-field representation of discretely sampled surface deformation for displacement and strain analysis", *Exp. Mech.*, **31**(2), 168-177. DOI: 10.1007/BF02327571.
- Wang, C.C., Deng, J.M., Ateshian, G.A. and Hung, C.T. (2002), "An automated approach for direct measurement of two-dimensional strain distributions within articular cartilage under unconfined compression", *J. Biomech. Eng.*, **124**(5), 557-567. DOI: 10.1115/1.1503795.
- Xu, Y.F. and Zhu, W.D. (2017), "Non-model-based damage identification of plates using measured mode shapes", *Struct. Health Monit.*, **16**(1), 3-23. DOI: 10.1016/j.jsv.2017.03.030.
- Xu, Y.F., Zhu, W.D. and Smith, S.A. (2017), "Non-model-based damage identification of plates using principal, mean and Gaussian curvature mode shapes", *J. Sound Vib.*, **400**, 626-659. DOI: 10.1016/j.jsv.2017.03.030.
- Ye, X.W., Dong, C.Z. and Liu, T. (2016), "Image-based structural dynamic displacement measurement using different multi-object tracking algorithms", *Smart Struct. Syst.*, **17**(6), 935-956. <http://dx.doi.org/10.12989/sss.2016.17.6.935>.
- Ye, X.W., Ni, Y.Q., Wai, T.T., Wong, K.Y., Zhang, X.M. and Xu, F. (2013), "A vision-based system for dynamic displacement measurement of long-span bridges: algorithm and verification", *Smart Struct. Syst.*, **12**(3-4), 363-379. http://dx.doi.org/10.12989/sss.2013.12.3_4.363.
- Ye, X.W., Yi, T.H., Wen, C. and Su, Y.H. (2015), "Reliability-based assessment of steel bridge deck using a mesh-insensitive structural stress method", *Smart Struct. Syst.*, **16**(2), 367-382. <http://dx.doi.org/10.12989/sss.2015.16.2.367>.
- Yuen, K.V. and Katafygiotis, L.S. (2003), "Bayesian fast Fourier transform approach for modal updating using ambient data", *Adv. Struct. Eng.*, **6**(2), 81-95. DOI: 10.1260/136943303769013183.
- Yuen, K.V. and Katafygiotis, L.S. (2001), "Bayesian time-domain approach for modal updating using ambient data", *Probab. Eng. Eng. Mech.*, **16**(3), 219-231. DOI: 10.1016/S0266-8920(01)00004-2.
- Yuen, K.V. and Katafygiotis, L.S. (2005), "Model updating using noisy response measurements without knowledge of the input spectrum", *Earthq. Eng. Struct. D.*, **34**(2), 167-187. DOI: 10.1002/eqe.415.
- Zanarini, A. (2018), "Broad frequency band full field measurements for advanced applications: Point-wise comparisons between optical technologies", *Mech. Syst. Signal Pr.*, **98**, 968-999. DOI: 10.1016/j.ymsp.2017.05.035.